Nanoscale



COMMUNICATION

View Article Online

High performance few-layer GaS photodetector and its unique photo-response in different gas environments†

Cite this: DOI: 10.1039/c3nr05965k

Received 9th November 2013 Accepted 2nd December 2013

DOI: 10.1039/c3nr05965k

www.rsc.org/nanoscale

Shengxue Yang,^a Yan Li,^a Xiaozhou Wang,^b Nengjie Huo,^a Jian-Bai Xia,^a Shu-Shen Li^a and Jingbo Li^{*a}

Layered GaS nanosheets have been attracting increasing research interests due to their highly anisotropic structural, electrical, optical, and mechanical properties, which are useful for many applications. However, single-layer or few-layer GaS-based photodetectors have been rarely reported. Here a few-layer GaS two-terminal photodetector with a fast and stable response has been fabricated. It shows different photo-responses in various gas environments. A higher photo-response (64.43 A W $^{-1}$) and external quantum efficiency (EQE) (12 621%) is obtained in ammonia (NH $_{\rm 3}$) than in air or oxygen (O $_{\rm 2}$). A theoretical investigation shows that the charge transfer between the adsorbed gas molecules and the photodetector leads to the different photo-responses.

1 Introduction

Two-dimensional (2D) materials have attracted significant attention from the scientific community, due to their potential exotic transport physics and prospects for various technological applications.¹ 2D materials-based nanodevices in electronic fields allow possible further miniaturization beyond Moore's Law and they can serve as a high-mobility option applied to large-area and low-cost electronic devices.²³ Graphene is the most widely studied 2D material so far because of its unusual electrical, magnetic, optical and mechanical properties.⁴⁴6 However, several problems remain with graphene due to absence of a bandgap, which is essential for many applications. For example, graphene can hardly be applied in photodetectors

metal atoms (M) sandwiched between two layers of chalcogen atoms (X) have been regarded as promising materials. Combining a chalcogen (X = S, Se, or Te) with a transition metal (M = Mo, W, Nb, Re, Ni, Ta, Ti, Zr, Hf or V), TMDs can form in dozens of different categories. TMDs with strong X-M-X intralayer covalent bonding within the layers and weak interlayer interaction (van der Waals in nature) have been studied with much attention in view of their great potential in many fields. The preparation, isolation and rapid characterization of layered GaS and other TMDs as well as their optical contrast on various Si/SiO₂ substrates have been reported. This was of benefit for the in-depth exploration and potential applications of TMDs. Developing novel photodetectors is of significant importance in the progress of the optoelectronics field. Among a crowd of

or photoswitching microdevices which need definite on-and-off

states.7 As analogues of graphene, layered transition metal

dichalcogenides (TMDs) consisting of one layer of transition

various photodetectors, the low dimensional materials-based photodetectors are very attractive because of their compact size and ease of manipulation. It is well known that low dimensional materials with large surface-to-volume ratio can yield higher photosensitivity than their bulk counterparts and the lifetime of photo-generated carriers is considerably prolonged because of charge separation.11 Some TMDs layered material photodetectors have been developed and much used in recent years, because of their easy to fabricate complex structures. GaS nanosheet photodetectors made on SiO₂/Si substrates and flexible polyethylene terephthalate (PET) substrates exhibit a photoresponsivity at 254 nm of up to 4.2 A W^{-1} and 19.2 A W^{-1} , respectively, which is better than some other 2D material based devices. 11,12 Lopez-Sanchez et al. demonstrated ultrasensitive monolayer MoS2 phototransistors which showed a maximum external photoresponsivity of 880 A W⁻¹ at a wavelength of 561 nm and a photo-response in the 400-680 nm range.8 This is due to their improved mobility, good contact quality and positioning technique. The high surface-to-volume ratio is also useful for new sensor materials which must exhibit selectivity to

[&]quot;State Key Laboratory of Superlattices and Microstructures, Institute of Semiconductors, Chinese Academy of Sciences, P.O. Box 912, Beijing 100083, China. E-mail: jbli@semi.ac.cn

^bZhejiang Provincial Key Laboratory of Solid State Optoelectronic Devices, Zhejiang Normal University, Zhejiang 321004, China

[†] Electronic supplementary information (ESI) available: Experimental section, density functional theory calculations, EDX of GaS nanosheet, I-t curve in O_2 gas environment and in vacuum, saturated I-t curve in NH_3 gas environment. See DOI: 10.1039/c3nr05965k

the analytes, rapid response and recovery, and sensitive transduction of the measured parameters without interference.3 Field-effect transistor (FET) sensors based on multilayer MoS₂ films exhibit a high sensitivity to NO with a detection limit of 0.8 ppm due to their large specific surface areas. 13 The MoS₂ transistors with different thicknesses have been assessed for gassensing performances with exposure to NO2, NH3, and humidity in different conditions such as gate bias and light irradiation.14

In recent years, considerable progress has been made for the fabrication of different layer-structured III-VI semiconductors in various forms via several techniques in a controlled manner, such as micromechanical cleavage, epitaxial growth, chemical vapor deposition, and liquid exfoliation.15-19 Various highquality GaS nanostructures as well as other kinds of GaS products have produced in a controlled synthesis via a simple vaporsolid method.¹⁶ Among the III-VI group of semiconductor materials, GaS is one of the most important materials. It has two different stoichiometries, i.e., GaS and Ga₂S₃. It is well known that hexagonal GaS has layered structures with each layer consisting of a S-Ga-Ga-S repeating unit built by six-membered Ga₃S₃ rings.²⁰ Layered GaS, with an indirect bandgap of 2.5 eV, is more useful for applications in photoelectric devices, electrical sensors, and nonlinear optical applications, owing to its highly anisotropic structural, electrical, optical, and mechanical properties.16 Doped GaS can be used for the fabrication of nearblue-light emitting devices. The photoluminescence yield for thin films of GaS deposited on a GaAs substrate are higher than that of GaAs.21 A single-sheet of GaS exhibits field-effect respective differential mobilities of ~0.1 cm² V⁻¹ s⁻¹ along with good on/off current ratios in the range of $\sim 10^4$ to 10^5 . However, comparable single-layer or few-layer GaS-based photodetectors have been rarely reported.

In this communication, we report the design of few-layer GaS photodetectors. The ultrathin GaS nanosheets mechanically exfoliated on a SiO₂/Si substrate are characterized by atomic force microscopy (AFM) and Raman spectroscopy. After deposition of Au electrodes, the two-terminal photodetectors are fabricated. The fabricated GaS photodetector shows different photo-responses in various gas environments. It has higher current on/off ratio, photo-response and EQE in an NH3 environment than in air or in O2. The photo-response time is around 10 ms, and it still shows good stability after dozens of switching cycles. The unique characteristics of prompt photoswitching, fast response time and good photoresponsivity from the GaS photodetector pave the way for the fabrication of multifunctional and high performance flexible photodetectors and gas sensors based on the layered semiconducting materials in the future.

2 Results and discussion

Crystals of GaS are composed of vertically stacked, weakly interacting layers held together by van der Waals interactions (Fig. 1a) and the thickness of a single layer is ~7.5 Å (Fig. 1b).¹¹ It has a stable, hexagonal, double-layered structure with bond distances of 2.48 Å and 2.37 Å for the Ga-Ga and Ga-S bond lengths, respectively.¹⁶ The micromechanical cleavage

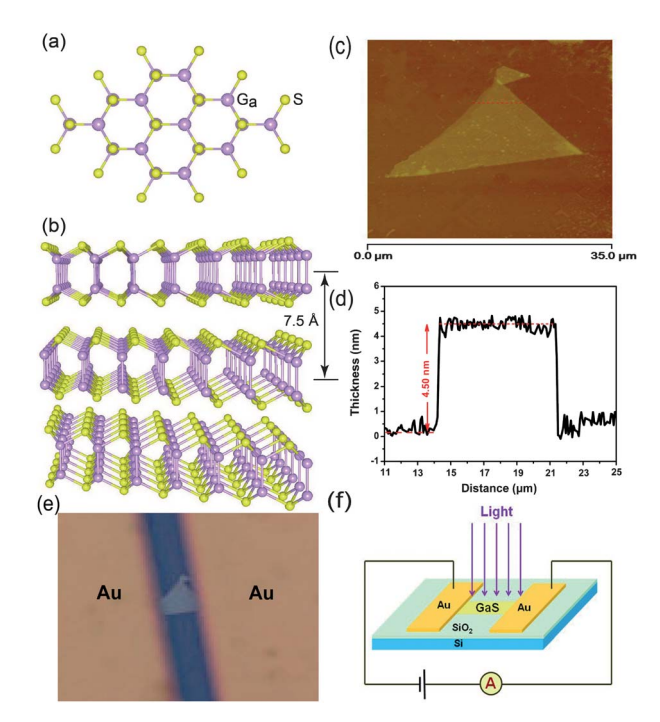


Fig. 1 (a) The top view and (b) side view of the GaS nanosheet, (c) AFM image and (d) a height profile of the few-layer GaS nanosheet, (e) optical image of the device and (f) schematic of the device operation.

technique has been used to fabricate different-layer GaS sheets by repeatedly peeling the bulk material and transferring this peeled material on top of a SiO₂/Si substrate using adhesive tape. This technique has been proven to be an easy and very fast way of producing highly crystalline and large size sheets of single and few layers.1 A few-layer nanosheet of GaS derived from micromechanical cleavage from bulk crystal of GaS is shown in Fig. 1c, corresponding to the AFM image of GaS few layers peeled on 300 nm SiO₂/Si substrates. A height profile along the dashed line in Fig. 1c is depicted in Fig. 1d. It is noted that the ultrathin GaS nanosheet has a thickness of 4.5 nm, indicating ~6 layers of GaS. As shown in Fig. 1e, a pair of Au electrodes (\sim 50 nm thick) with 28 μ m apart are evaporated by laying a micrometer-sized diametral Au wire as the mask on top of the few-layer GaS peeled on a Si substrate with a 300 nm SiO₂ insulating top layer to obtain a gap between the two electrodes. After the evaporation of the electrodes, the Au wire mask is removed so that the sample in the gap area can be exposed.

Raman spectroscopy is a convenient tool for nondestructive characterization and identification of few-layer materials. Three phonon modes exist in the first-order Raman spectroscopy of GaS nanosheet, *i.e.* A_{1g}^1 , E_{2g}^1 , and A_{2g}^1 as shown in Fig. 2a. Fig. 2b shows the comparative Raman spectra of bulk and the few-layer of GaS. Typically bulk GaS shows Raman modes A_{1g} (186.89 cm^{-1}) , E_{2g}^1 (288.91 cm^{-1}) , and A_{2g}^1 (368.37 cm^{-1}) . The frequency shifts of the few-layer GaS Raman modes at room temperature are found to be A_{1g}^1 (183.41 cm⁻¹), E_{2g}^1 (297.35 cm^{-1}) , and A_{1g}^2 (365.28 cm^{-1}) . As shown in Fig. 2a, the frequency of the E_{2g}^1 mode of few-layer GaS increases and that of A_{1g}^1 and A_{2g}^1 mode decreases, which corresponds well with the

Communication Nanoscale

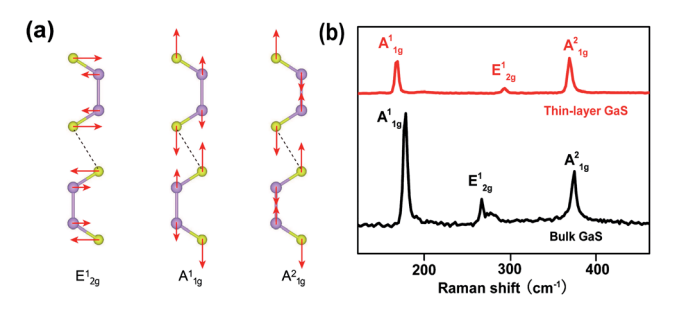


Fig. 2 (a) Schematic illustration of phonon modes in first-order Raman spectroscopy, and (b) Raman spectroscopy of bulk and fewlayer GaS.

reported Raman spectrum in the ultrathin GaS nanosheet.¹¹ The energy-dispersive X-ray spectrum (EDX) is used to analyze the composition of the few-layer GaS nanosheet, as shown in Fig. S1 (ESI).†

β-phase GaS with an experimental lattice constant a = 3.585Å is used for band structure calculations,22 as illustrated in Fig. 1. The calculated band structures of GaS bulk and nanosheets of monolayer, 3-layer and 6-layer are shown in Fig. 3. The valence band maximum (VBM) and conduction band minimum (CBM) of GaS bulk are located at the Γ and M points, respectively, resulting an indirect bandgap of 1.61 eV, agreeing with previous theoretical results.11 An interesting change occurs to the VBM when GaS undergoes a dimensionality change. The VBM slightly moves along the Γ -K direction for nanosheets from the monolayer to 5-layer with the energy difference between the VBM and Γ point within 0.11 eV. The CBMs of the nanosheets are located at the M point without change. For the GaS monolayer, the bandgap is 2.59 eV, consistent with previous work. 11 The second CBMs of GaS are located at Γ with a small energy difference between the second VBM and VBM less than 0.16 eV, therefore, a great direct Γ – Γ transition probability can be expected.

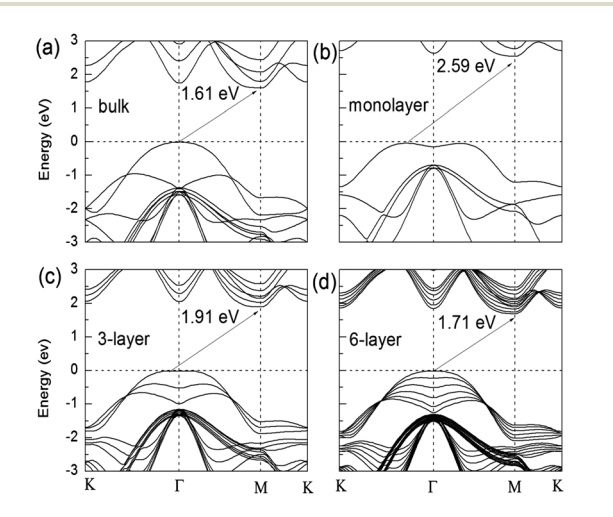


Fig. 3 The calculated band structures of GaS (a) bulk and nanosheets of (b) monolayer, (c) 3-layer and (d) 6-layer.

We probed the devices (Fig. 1f) and their time-dependent photo-response to laser excitation using a focused laser beam ($\lambda = 633$ nm) as an irradiation source under different gas environments (NH3, air and O2). Before we filled the measurement system with NH3 or O2, the test system was firstly evacuated to exclude interference from other gases in air. The power of the light could be controlled from ~ 106.5 to 189.8 μW cm⁻². The bias voltage between two electrodes was kept constant at 1 V. Fig. 4a displays the photocurrent versus time plots of the device irradiated by 633 nm light with a light intensity of 189.8 μ W cm⁻² in air and an NH₃ gas environment, respectively. The irradiation source was switched on and off periodically at 10 s intervals. From the curve, it could be seen that the device exhibited excellent photo-response properties. Under an air environment, the dark current was around 1.5 nA. However, under red light irradiation, the photocurrent could approach 28 nA with a current on/off ratio of around 18.6. In an NH₃ environment, the dark current was \sim 2 nA, the photocurrent was 48 nA and the on/off ratio was around 24. We have also measured the photo-response in an O2 gas environment, the dark current was <1 nA, then after irradiation by light, a photocurrent jump of \sim 7 nA was obtained. However, in

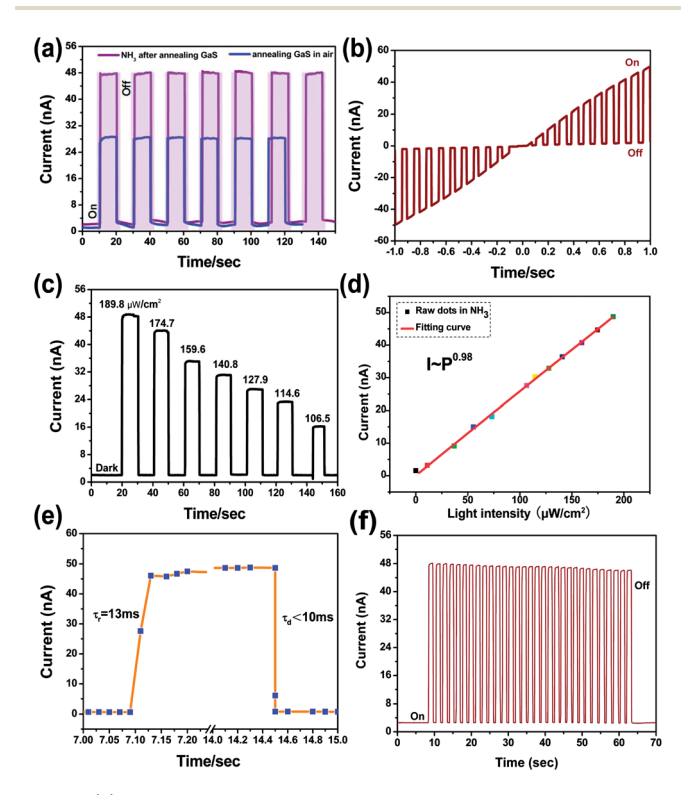


Fig. 4 (a) Time-resolved photocurrent of the photodetector in response to light on/off in different gas environments (the bias voltage between two electrodes is kept constant at 1 V), (b) $I\!-\!V$ curve when the photodetector is alternately illuminated with 633 nm light on/off at an irradiance of 189.8 μW cm $^{-2}$ in NH $_3$ gas, (c) the photocurrent–time curve with the change of light intensity, (d) experimental data fitting of photocurrent–time curve with the change of light intensity, (e) the photocurrent responses with time under illumination of 633 nm in an NH $_3$ environment and (f) representative switching cycles in NH $_3$ with 1 V bias when a 633 nm laser was switched on and off repeatedly.

vacuum, the photo-response was higher than that in air (as shown in ESI, Fig. S2).† The photocurrent intensity and current on/off ratio in NH3 was much higher than that in air or in O2. And for NH₃ gas environment, with the light irradiation on and off, the photo-response displayed three transient regimes: a sharp rise, steady state, and sharp decay. The current increased very sharply from one state to another state, indicating a very fast response speed of the device. When irradiated by red light in NH₃, the photocurrent quickly increased to a saturated value of 50 nA, and then dramatically decreased to its initial value when the light was turned off (ESI Fig. S3).† The current-voltage (I-V) characteristic measured by switching on/off the red light (189.8 μ W cm⁻²) in NH₃ is shown in Fig. 4b. Connecting the curves in dark and/or under light illumination, respectively, we noted that both I-V curves in dark and under light illumination were nearly linear, which indicated a good Ohmic contact. The relationship between the photocurrent ($I_{\rm photo} = I_{\rm light} - I_{\rm dark}$) and the light intensity was also investigated. Fig. 4c shows that the photocurrent increased in a step-like manner as the light intensity was enhanced. The photocurrent was linearly proportional to the incident irradiation intensity within the range of \sim 106.5 to 189.8 μ W cm⁻². Within the linear range, the few-layer GaS nanosheet should be a typical photon-dependent resistor in that more photons would generate more photocarriers.23,24 The experimental data of photocurrent-time curve could be best fit by using the power law $I_{\text{photo}} = AP_{\lambda}^{\beta}$, where A was the proportionality constant; β was an exponent that determined the response of I_{photo} to the incident light intensity (P_{λ}) . Under an NH₃ environment, I_{photo} exhibited a intensity dependence of \sim 0.98 as shown in Fig. 4d, indicating a highly efficient generation of carriers transferred from photons. Response time and repeatability are also key parameters to determine the capability of a photodetector. It is still a challenge to achieve photodetectors with both high photosensitivity and fast lasting response to date. Fig. 4e shows the photoresponse of the device under the illumination (633 nm and 189.8 μ W cm⁻²) in an NH₃ environment. The dynamic response to the light illumination for rise and decay could be expressed by $I(t) = I_0 \left[1 - \exp(-t/\tau_r) \right]$ and $I(t) = I_0 \exp(-t/\tau_d)$, where τ_r and $\tau_{\rm d}$ were the time constants for the rise and decay edges, respectively.^{25,26} We noted that the photocurrent rise and decay for our device were very steep; τ_r and τ_d could be estimated to be 13 and \sim 10 ms, respectively. Representative switching cycles in

The photoresponsivity (R_{λ}) and the EQE are both critical parameters for photodetectors, which determine sensitivity for an optoelectronic device. R_{λ} was defined as the photocurrent generated per unit power of incident light on the effective area of a photodetector. EQE was defined as the number of carriers circulating through a photodetector per adsorbed photon and per unit time, R_{λ} and EQE could be calculated in the following equations: $R_{\lambda} = \Delta I_{\lambda}/(P_{\lambda}S)$ and EQE $= hcR_{\lambda}/(e\lambda)$, where $\Delta I_{\lambda} = I_{\text{light}} - I_{\text{dark}}$ was the photocurrent, S was the effective illuminated

NH₃ with 1 V bias when a 633 nm laser was switched on and off repeatedly are shown in Fig. 4f. After multiple illumination

cycles, the photocurrent still responded in a similar fashion to

the light, which demonstrated the high robustness and good

reproducibility of the photodetectors.

area, h was Planck's constant, c was the light velocity, e was the electronic charge, and λ was the incident light wavelength. 23,26,27 For our device, $\Delta I_{\lambda}=4.6\times10^{-8}$ A, $P_{\lambda}=189.8~\mu\mathrm{W}~\mathrm{cm}^{-2}$, $S=\sim376.32~\mu\mathrm{m}^2$, $\lambda=633~\mathrm{nm}$, then R_{λ} and EQE could be estimated to be about 64.43 A W⁻¹ and 12 621%, respectively. The parameters of the GaS photodetector compared to other optoelectronic devices are shown in Table 1. The photo-response of our device was higher than the pure monolayer graphene photodetector (8.61 A W⁻¹)³² and graphene nanoribbons (1 A W⁻¹). But the response time was still slower than the graphene photodetectors. And graphene based device had a broad operation spectrum (from 1.35 to 1.6 mm) under ambient conditions.

To investigate the influence of gas adsorption on photosensitivity, the interactions between the GaS monolayer and NH₃ or O₂ were simulated using first-principles calculations. Extensive tests of the adsorbing positions and the gap molecular configurations revealed that $NH_3(O_2)$ was physisorbed above the Ga atom on the monolayer with a 156.1 meV (102.55 meV) binding energy. Approximately, 0.02 electrons per NH₃ were transferred from NH₃ to the GaS monolayer, while 0.07 electrons per O₂ were transferred from the GaS monolayer to O2, therefore, NH3 served as the donor but O2 acted as the acceptor. Moreover, the transferred charges were more localized around adsorbed O2 than adsorbed NH3, which is demonstrated in Fig. 5. Brown denotes charge accumulation in O2 and green denotes charge depletion in NH₃ (Fig. 5). This proves that NH₃ lost electrons to GaS and O2 captured electrons from GaS. To enhance the sensitivity to the gas environment, an annealing process was needed for the few-layer GaS nanosheet. Here, the annealing could be applied to thermally drive away contaminants/organic residue, simultaneously, it might be creating a small density of chalcogen vacancies.28 After the annealing process, the photocurrent intensity of the nanosheet became extremely sensitive to the gas environment as shown in Fig. 4. We also calculated the charge transfer under the NH3 environment after the generation of chalcogen vacancies. The result showed that 0.12 electrons per NH3 were transferred from NH3 to the GaS monolayer. And after the generation of chalcogen vacancies, the structure of the GaS changed, resulting in an increase of the adsorption energy, a decrease of the distance between NH3 molecule and GaS monolayer, and an enhancement of the charge transfer from NH₃ to GaS (shown in ESI Fig. S4).† Since the mechanically exfoliated GaS nanosheet was an n-type semiconductor with background free electrons coming probably from defects, the adsorption of NH3 further transferred

Table 1 Comparison of the parameters of few-layer GaS device to the reported 2D material based photodetectors

Photodetectors	$R_{\lambda} (A W^{-1})$	EQE (%)	Response time
Few-layer MoS ₂ ³⁰	0.57		$\sim \mu s$
Graphene ³¹	1.0×10^{-3}	6-16	
Monolayer graphene ³²	8.61		\sim 200 s
Few-layer GaSe sheets ³⁶	2.8	1367	\sim 0.02 s
Our photodetector	64.43	12 621	\sim 10 ms
Few-layer GaSe sheets ³⁶	2.8		\sim 0.02 s

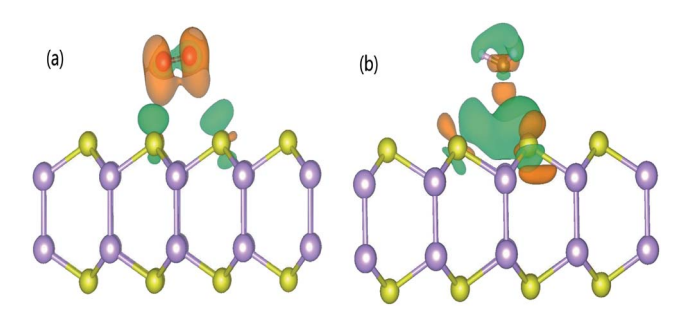


Fig. 5 A gas molecule adsorbed on the GaS monolayer. The charge density difference between pristine GaS and (a) O_2 -adsorbed and (b) NH_3 -adsorbed GaS monolayer. The iso-surface is for an electron density of 6×10^{-4} e Å⁻³. Brown denotes charge accumulation and green denotes charge depletion.

electrons to the nanosheet and increased its carrier density.28,29 When irradiated by light, the GaS nanosheet strongly absorbed the photons, and electron-hole pairs generated in the nanosheet. Under the external electric field, the photogenerated carriers moved and were separated, resulting in the generation of the photocurrent. When the device was used in an NH₃ environment, the adsorption of NH3 could increase the carrier density of the GaS nanosheet due to electron transfer, so we noted that the photo-response in NH₃ gas was better than that in air (Fig. 4b). But when measured in O2, because of the reversed electron transfer from GaS to O2 and the decrease of carrier density, the photo-response of the device was greatly weakened. Therefore, the device exhibited much better photosensitive properties in an NH3 environment than that in air or O2. And for vacuum, there was no interference from adsorbed gases (like O₂) or electron transfer between the surrounding environment and GaS nanosheet, so the photocurrent was higher than that in air.

3 Conclusions

In summary, high performance few-layer GaS nanosheet photodetectors have been fabricated. The R_{λ} and EQE of the device were obtained at different gas environments and exhibited $\sim\!64.43~{\rm A~W^{-1}}$ and 12 621%, respectively, under 633 nm light irradiation in an NH $_3$ environment. The switching cycles of photocurrent were fast and stable. A theoretical investigation of the effect of NH $_3$ and/or O $_2$ adsorption on the photo-response was also performed. These experimental and theoretical findings indicated that the few-layer GaS nanosheet could be used in high-performance nanosensors, photodetectors, photoswitches and optoelectronic circuits.

Acknowledgements

We thank Prof. Junqiao Wu and Dr Sefaattin Tongay for the discussion. Prof. Jingbo Li gratefully acknowledges financial support from National Science Found for Distinguished Young Scholar (Grant no. 60925016 and 91233120) and the National Basic Research Program of China (Grant no. 2011CB921901). Dr

Shengxue Yang acknowledges financial support from China Postdoctoral Science Foundation (no. 2013M540127).

Notes and references

- D. J. Late, B. Liu, J. Luo, A. Yan, H. S. S. R. Matte,
 M. Grayson, C. N. R. Rao and V. P. Dravid, *Adv. Mater.*,
 2012, 24, 3549.
- 2 H. Wang, L. Yu, Y. Lee, Y. Shi, A. Hsu, M. L. Chin, L. Li, M. Dubey, J. Kong and T. Palacios, *Nano Lett.*, 2012, 12, 4674.
- 3 F. K. Perkins, A. L. Friedman, E. Cobas, P. M. Campbell, G. G. Jernigan and B. T. Jonker, *Nano Lett.*, 2013, **13**, 668.
- 4 A. K. Geim and K. S. Novoselov, Nat. Mater., 2007, 6, 183.
- 5 A. K. Geim, Science, 2009, 324, 1530.
- 6 C. N. R. Rao, A. K. Sood, K. S. Subrahmanyam and A. Govindaraj, *Angew. Chem., Int. Ed.*, 2009, **48**, 7752.
- 7 H. S. Lee, S. Min, Y. Chang, M. K. Park, T. Nam, H. Kim, J. H. Kim, S. Ryu and S. Im, *Nano Lett.*, 2012, 12, 3695.
- 8 O. Lopez-Sanchez, D. Lembke, M. Kayci, A. Radenovic and A. Kis, *Nat. Nanotechnol.*, 2013, **8**, 497.
- 9 M. Xu, T. Liang, M. Shi and H. Chen, *Chem. Rev.*, 2013, **113**, 3766.
- 10 D. J. Late, B. Liu, H. S. S. Ramakrishna Matte, C. N. R. Rao and V. P. Dravid, *Adv. Funct. Mater.*, 2012, 22, 1894;
 V. Stengl and J. Henych, *Nanoscale*, 2013, 5, 3387;
 W. Ge, K. Kawahara, M. Tsuji and H. Ago, *Nanoscale*, 2013, 5, 5773.
- 11 P. Hu, L. Wang, M. Yoon, J. Zhang, W. Feng, X. Wang, Z. Wen, J. C. Idrobo, Y. Miyamoto, D. B. Geohegan and K. Xiao, *Nano Lett.*, 2013, 13, 1649.
- 12 Z. Yin, H. Li, L. Jiang, Y. Shi, Y. Sun, G. Lu, Q. Zhang, X. Chen and H. Zhang, *ACS Nano*, 2012, **6**, 74.
- 13 H. Li, Z. Yin, Q. He, H. Li, X. Huang, G. Lu, D. W. H. Fam, A. I. Y. Tok, Q. Zhang and H. Zhang, *Small*, 2012, **8**, 63.
- 14 D. J. Late, Y. Huang, B. Liu, J. Acharya, S. N. Shirodkar, J. Luo, A. Yan, D. Charles, U. V. Waghmare, V. P. Dravid and C. N. R. Rao, *ACS Nano*, 2013, 7, 4879.
- 15 K. S. Novoselov, A. K. Geim, S. V. Morozov, D. Jiang, Y. Zhang, S. V. Dubonos, I. V. Grigorieva and A. A. Firsov, *Science*, 2004, 306, 666.
- 16 G. Shen, D. Chen, P. Chen and C. Zhou, ACS Nano, 2009, 3, 1115.
- 17 C. Berger, Z. Song, T. Li, X. Li, A. Y. Ogbazghi, R. Feng, Z. Dai, A. N. Marchenkov, E. H. Conrad, P. N. First and W. A. de Heer, *J. Phys. Chem. B*, 2004, **108**, 19912.
- 18 R. Rosei, S. Modesti, F. Sette, C. Quaresima, A. Savoia and P. Perfetti, *Phys. Rev. B: Condens. Matter Mater. Phys.*, 1984, 29, 3416; Y. C. Lin, W. Zhang, J. K. Huang, K. K. Liu, Y. H. Lee, C. T. Liang, C. W. Chud and L. J. Li, *Nanoscale*, 2012, 4, 6637.
- 19 J. N. Coleman, M. Lotya, A. O'Neill, S. D. Bergin, P. J. King, U. Khan, K. Young, A. Gaucher, S. De, R. J. Smith, I. V. Shvets, S. K. Arora, G. Stanton, H. Kim, K. Lee, G. T. Kim, G. S. Duesberg, T. Hallam, J. J. Boland, J. J. Wang, J. F. Donegan, J. C. Grunlan, G. Moriarty, A. Shmeliov, R. J. Nicholls, J. M. Perkins, E. M. Grieveson,

Nanoscale

- 20 G. Sinha, S. K. Panda, A. Datta, P. G. Chavan, D. R. Shinde, M. A. More, D. S. Joag and A. Patra, ACS Appl. Mater. Interfaces, 2011, 3, 2130.
- 21 T. Aono, K. Kase and A. Kinoshita, J. Appl. Phys., 1993, 74, 2818; Q. S. Xin, S. Conrad and X. Y. Zhu, Appl. Phys. Lett., 1996, 69, 1244.
- 22 H. Damour, W. B. Holzapfel, A. Polian and A. Chevy, *Solid State Commun.*, 1982, 44, 853.
- 23 Z. Wang, M. Safdar, C. Jiang and J. He, *Nano Lett.*, 2012, 12, 4715.
- 24 Q. L. Li, Y. Li, J. Gao, S. D. Wang and X. H. Sun, *Appl. Phys. Lett.*, 2011, **99**, 243105.
- 25 Y. Liang, H. Liang, X. Xiao and S. Hark, *J. Mater. Chem.*, 2012, **22**, 1199.
- 26 Y. Zhang, W. Deng, X. Zhang, X. Zhang, X. Zhang, Y. Xing and J. Jie, ACS Appl. Mater. Interfaces, 2013, 5, 12288.
- 27 L. Hu, J. Yan, M. Liao, H. Xiang, X. Gong, L. Zhang and X. Fang, *Adv. Mater.*, 2012, **24**, 2305.

- 28 S. Tongay, J. Zhou, C. Ataca, J. Liu, J. S. Kang, T. S. Matthews, L. You, J. Li, J. C. Grossman and J. Wu, *Nano Lett.*, 2013, 13, 2831.
- 29 S. Y. Hu, Y. Z. Chen, K. K. Tiong and Y. S. Huang, *Mater. Chem. Phys.*, 2007, **104**, 105; Q. Yue, Z. Shao, S. L. Chang and J. Li, *Nanoscale Res. Lett.*, 2013, **8**, 425.
- 30 D. Tsai, K. Liu, D. Lien, M. Tsai, C. Kang, C. Lin, L. Li and J. He, *ACS Nano*, 2013, 7, 3905.
- 31 F. Xia, T. Mueller, Y. Lin, A. Valdes-Garcia and P. Avouris, *Nat. Nanotechnol.*, 2009, 4, 839.
- 32 Y. Zhang, T. Liu, B. Meng, X. Li, G. Liang, X. Hu and Q. Wang, *Nat. Commun.*, 2013, 4, 1811.
- 33 B. Chitara, L. S. Panchakarla, S. B. Krupanidhi and C. N. R. Rao, *Adv. Mater.*, 2011, 23, 5419.
- 34 A. Urich, K. Unterrainer and T. Mueller, *Nano Lett.*, 2011, **11**, 2804.
- 35 M. Liu, X. Yin, E. Ulin-Avila, B. Geng, T. Zentgraf, L. Ju, F. Wang and X. Zhang, *Nature*, 2011, 474, 64.
- 36 P. Hu, Z. Wen, L. Wang, P. Tan and K. Xiao, *ACS Nano*, 2012, **6**, 5988.